

# Effects of Cold Eddy on Kuroshio Meander and Its Surface Properties, East of Taiwan

Po-Chun Hsu, *Student Member, IEEE*, Chen-Chih Lin, Shih-Jen Huang, and Chung-Ru Ho

**Abstract**—Satellite remote-sensing data and glider data are used to study the Kuroshio meander and surface properties, east of Taiwan. The Kuroshio meandered eastward 13 times between 1993 and 2013 because of cold eddies propagating from the western Pacific. The maximum duration of the meanders was 80 days. The farthest eastward shift of the Kuroshio axis was approximately 270 km from its original position, depending on the size of the cold eddy. Cold eddies reduce the current speed at the Kuroshio axis to 84% of its seasonal average, which is approximately 0.75 m/s. According to glider data, isopycnal uplifting is produced when cold eddies impinge on the Kuroshio, and satellite observations show that the sea surface temperature (SST) drops 1–3 °C and that the chlorophyll-a (chl-a) concentration increases up to 0.54 mg/m<sup>3</sup>.

**Index Terms**—Chlorophyll-a (chl-a), cold eddy, kuroshio meander, sea surface temperature (SST).

## I. INTRODUCTION

THE KUROSHIO, a western boundary current (WBC) in the North Pacific, originates from the North equatorial current and flows northward east of Luzon and Taiwan. Previous studies have shown that this is an eddy-rich zone, with eddies having been frequently observed for many years [1]–[3]. It is located in the North Pacific subtropical counter-current region (18 °N – 25 °N, 122 °E – 160 °E), near the center of the western subtropical gyre [4]. Mesoscale eddies from the interior ocean arrive east of Luzon [5] and Taiwan [6] (Fig. 1), where they impinge on the Kuroshio for approximately 100-day intervals [6]–[8005D and may cause the Kuroshio axis to shift and alter the velocity of the Kuroshio. Using moored current meter arrays, satellite altimeter data, and numerical model outputs, Zhang *et al.* [8] showed a close relationship between the impinging of mesoscale eddies and Kuroshio volume transport. Kuo and Chern [9] indicated that the gradient of relative vorticity to the east of the WBC is a crucial factor in the interaction between eddies and the WBC. Furthermore, Lien *et al.*

Manuscript received September 23, 2015; revised January 29, 2016; accepted January 29, 2016. Date of publication February 17, 2016; date of current version November 09, 2016. This work was supported in part by the Ministry of Science and Technology of Taiwan under Grant MOST 104-2611-M-019-020 and Grant MOST 104-2221-E-019-033, and in part by the National Natural Science Foundation of China under project U1405233.

P.-C. Hsu, C.-C. Lin, and S.-J. Huang are with the Department of Marine Environmental Informatics, National Taiwan Ocean University, Keelung 20224, Taiwan (e-mail: gingshu@gmail.com; mikania.lin@gmail.com; huangs@ntou.edu.tw).

C.-R. Ho is with the Department of Marine Environmental Informatics, National Taiwan Ocean University, Keelung 20224, Taiwan, and also with the National Museum of Marine Science and Technology, Keelung 20224, Taiwan (e-mail: b0211@mail.ntou.edu.tw).

Color versions of one or more of the figures in this paper are available online at <http://ieeexplore.ieee.org>.

Digital Object Identifier 10.1109/JSTARS.2016.2524698

[5] suggested that the Kuroshio transport is modulated near its origin by the impinging of mesoscale eddies. Eddy-induced vorticity near the Kuroshio has a similar seasonal cycle to that of mesoscale eddies. Takahashi *et al.* [10] used long-range, high-frequency radar to determine the variation in the Kuroshio axis off northeastern Taiwan. They found that the variation was caused by eddies propagating along the shelf slope from the deep ocean. Thus, facts regarding the Kuroshio variation affected by ocean eddies have been clearly shown. However, the scope of their influence and their effect on the surface properties of the Kuroshio remain unclear.

Sea-level anomalies (SLAs) derived from satellite altimetry have exhibited a favorable correlation with dynamic heights derived from temperature and salinity profiles [11]. Generally, a positive SLA corresponds to a depressed pycnocline, and a negative SLA corresponds to a lifting pycnocline. Thus, SLAs have been widely used for detecting ocean eddies [3], [12]–[14]. Zheng *et al.* [15] analyzed SLA data and determined that eddies originate from the west Pacific and sink into the South China Sea. Cheng *et al.* [16] found that the background current can affect an eddy pathway.

Satellite observations of sea surface properties, such as sea surface temperature (SST) and upper layer chlorophyll-a concentration (chl-a), are also largely applied to studying oceanic phenomena [17], [18]. The occurrence of a cyclonic eddy can drive water upwelling and cause SST drops, and chl-a increases in the upper ocean [19]. For example, Gu *et al.* [20] used SST images from a moderate-resolution imaging spectroradiometer (MODIS) to estimate upwelling vertical and horizontal velocities. Sarangi *et al.* [21] determined the impact of cyclones on phytoplankton distribution in the Bay of Bengal from chl-a data derived from MODIS and Oceansat-2 Ocean colour monitor (OCM) data sets.

The aforementioned studies indicate that remotely sensed satellite data are suitable for observing sea surface changes affected by eddies. Therefore, SLA and absolute dynamics topography (ADT) data derived from satellite altimetry and SST and chl-a data derived from MODIS measurements were used in this study to investigate variations in the Kuroshio axis and surface properties caused by impinging mesoscale eddies east of Taiwan.

## II. DATA AND METHODS

### A. Altimetry Data

This study used SLA and ADT data from 1993 to 2013, which were provided by the archiving validation and interpretation of satellite data in oceanography and the Centre

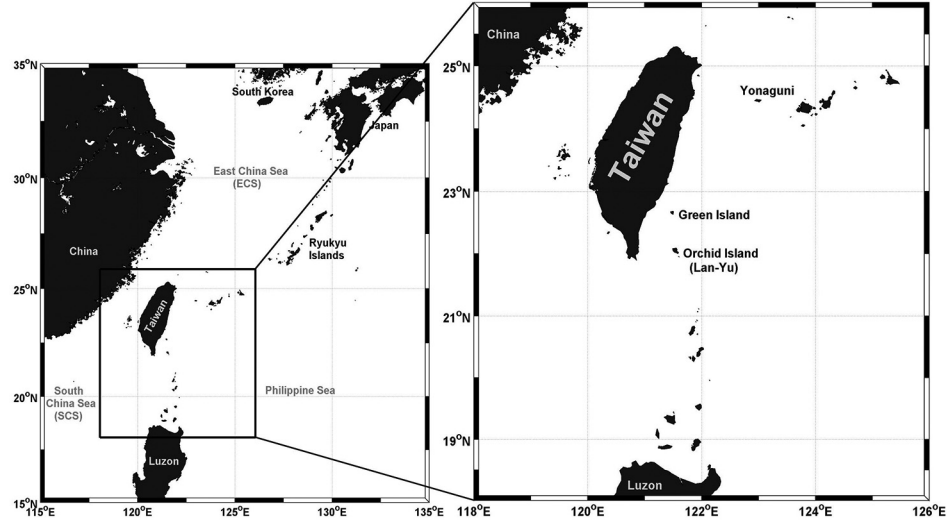


Fig. 1. Map of study area.

National d'Études Spatiales of France. ADT is defined as the sea surface height above the geoid and is obtained by summing the SLA and mean dynamic topography, which is derived from multivariate objective analysis. SLA and ADT data are merged by multiple satellite altimeters onboard the ERS-1/2, Envisat, TOPEX/Poseidon, and Jason-1/2 satellites. In this study, SLAs were used to detect eddies, and ADT was used to derive the absolute velocity. Although tidal and inverted barometer height corrections have been incorporated, the altimetry data in shallow-water applications are contaminated by full sea-level aliasing problems [22]. Thus, the altimetry data for shelf areas with water depths of less than 200 m were excluded.

### B. MODIS Data

The MODIS is a scientific instrument onboard the Terra and Aqua satellites. This instrument has 36 spectral bands ranging from 0.4 to 14.4  $\mu\text{m}$  in wavelength and at varying spatial resolutions (2 bands at 250 m, 5 bands at 500 m, and 29 bands at 1 km). Together the instruments provide SST and chl-a images of the entire earth every 1 to 2 days. Both SST and chl-a data used in this study are level-3 products, which are collected at a 4-km spatial resolution. These data were employed to examine changes in SST and chl-a concentration during the period of eddies impinging on the Kuroshio.

### C. Spray Glider Data

A glider is an autonomous underwater vehicle, which uses small changes in its buoyancy and wings to convert vertical motion to horizontal, thus propelling itself forward. It records its position by rolling on its side to expose a global positioning system (GPS) antenna and uses a compass and altitude sensors to control the pitch and roll of the glider to steer to target positions. Because of its low power consumption, a glider can measure ocean properties for an extended period and a long range even under unfavorable ocean conditions. This study used

data provided by the World ocean database to investigate upper layer variations in the Kuroshio when it is impinged by eddies.

### D. HYCOM Outputs

In addition to the remote-sensing data, model outputs from the hybrid coordinate ocean model (HYCOM) and navy coupled ocean data assimilation are also applied to this study. HYCOM is a numerical model interpolated to 40 standard z levels. The HYCOM outputs assimilate satellite altimeter observations and *in situ* vertical temperature and salinity profiles from expendable bathythermographs, Argo floats, and moored buoys. Outputs including the sea-level elevation, temperature, salinity, and velocity can be used for further validating the effects of eddies impinging on the Kuroshio.

## III. RESULTS

### A. Seasonal Variation in Kuroshio Axis

The Kuroshio axis is defined as the line with the maximum surface velocity along the Kuroshio path. The absolute geostrophic velocity is calculated from ADT data using the geostrophic relations

$$u = -\frac{g}{f} \frac{\partial \eta}{\partial y} \quad (1)$$

$$v = \frac{g}{f} \frac{\partial \eta}{\partial x} \quad (2)$$

where  $u$  and  $v$  are zonal and meridional velocity components, respectively;  $g$  is gravitational acceleration;  $f$  is the Coriolis parameter; and  $\eta$  is the ADT.

The seasonally averaged locations of the Kuroshio axis from 18 °N to 26 °N and from 1993 to 2013 are shown in Fig. 2(a). The Kuroshio axis east of Taiwan shows similar patterns in the four seasons. The pattern differences and changes in current speed were interpreted at each half-degree latitude from 22 °N to 25 °N (Table I). The Kuroshio axis deviates from the shore

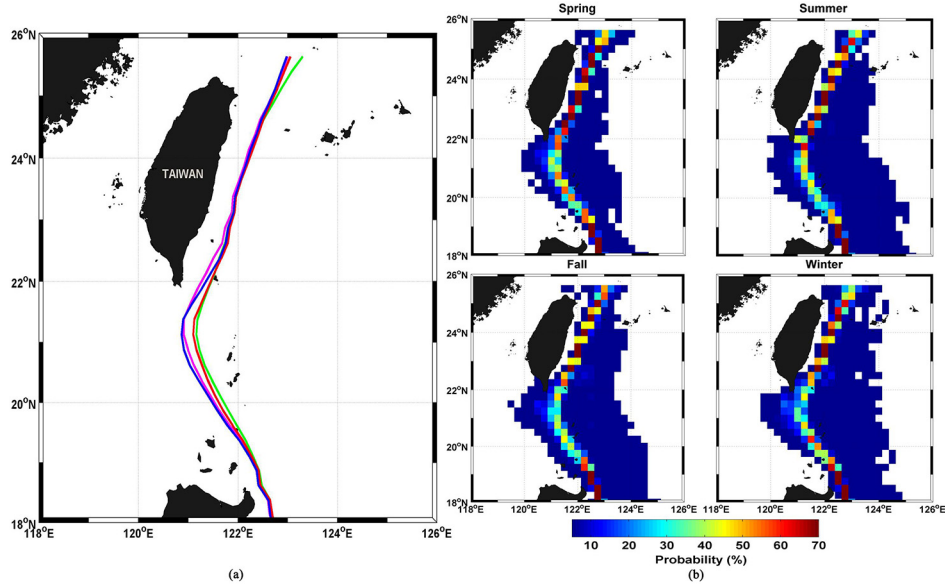


Fig. 2. (a) Seasonally averaged locations of Kuroshio axis from 18 °N to 26 °N and from 1993 to 2013, spring (magenta), summer (green), fall (red), and winter (blue). (b) Probability distribution of seasonal changes in the Kuroshio axis.

TABLE I  
AXIS POSITION AND SPEED (V) OF KUROSHIO IN FOUR SEASON

	Spring		Summer		Fall		Winter	
	Lon (°E)	V (m/s)						
22.0°N	121.27	0.60	121.46	0.70	121.45	0.53	121.36	0.50
22.5°N	121.59	0.63	121.68	0.74	121.73	0.59	121.70	0.55
23.0°N	121.81	0.80	121.86	0.86	121.89	0.75	121.86	0.71
23.5°N	121.96	0.86	122.00	0.91	122.01	0.77	121.99	0.75
24.0°N	122.17	0.83	122.21	0.88	122.23	0.73	122.20	0.70
24.5°N	122.40	0.84	122.46	0.93	122.46	0.79	122.42	0.73
25.0°N	122.69	0.90	122.79	0.97	122.72	0.81	122.69	0.72
Mean	121.98	0.78	122.07	0.86	122.07	0.71	122.03	0.67

in summer (June to August) and fall (September to November) and approaches the shore in winter (December to the following February) and spring (March to May). The average speed is faster in summer and slower in winter. The probability ( $p$ ) distribution of the seasonal changes in the Kuroshio axis that are shown in Fig. 2(b) is calculated using

$$p = \frac{N}{D} \times 100\% \quad (3)$$

where  $N$  is the number of Kuroshio axial positions that flow through the grid and  $D$  is the total number of data values. The Kuroshio axis changes significantly between 21 °N and 22 °N. The Kuroshio intrudes into the SCS in all seasons but interlopes the most in winter. In addition, the dark blue (< 5%) area on the right side of the Kuroshio axis occupies a larger portion than that on the left side; it could be caused by the effects of eddy interference.

#### B. Effects on Kuroshio Upper Layer

The data for two spray gliders were used to investigate the upper layer variations in the Kuroshio at 23 °N. Fig. 3 shows the case of a normal situation. Fig. 3(a) shows the Kuroshio axis

and its left boundary on an SLA map of January 28, 2012. The left boundary is defined as a line with the maximum gradient of the sea temperature at a depth of 200 m. In a normal situation, the SLA values are between -0.1 and 0.1 m [Fig. 3(b)]. A high speed of approximately 0.6 m/s occurs at the Kuroshio axis of 121.875 °E [Fig. 3(c)]. Comparisons of temperature-depth, salinity-depth, and density-depth profiles from spray glider data and HYCOM outputs are shown in Fig. 3(d). The high temperature area ( $> 24^{\circ}\text{C}$ ) appeared along the Kuroshio path. Abrupt temperature changes near the shoreline were caused by the mixing of coastal water. However, the surface salinity of the glider data is lower than that of the HYCOM outputs [white circle on Fig. 3(d)]. Tropical rainfall measuring mission/TRMM microwave imager data showed that then a heavy rainfall occurred. This implies that the HYCOM outputs had difficulty collecting timely conditions; the value gap between the two data sets is approximately 0.5 psu.

A case of a cold eddy impinging on the Kuroshio region is shown in Fig. 4. Fig. 4(a) shows the positions of the eddy and the Kuroshio on an SLA map of April 30, 2012. The center of the cold eddy was located near 23 °N, 123.3 °E, where the SLA decreased to -0.3 m [Fig. 4(b)] and the highest current speed was 1 m/s [Fig. 4(c)] near 123.6 °E. Fig. 4(d) shows

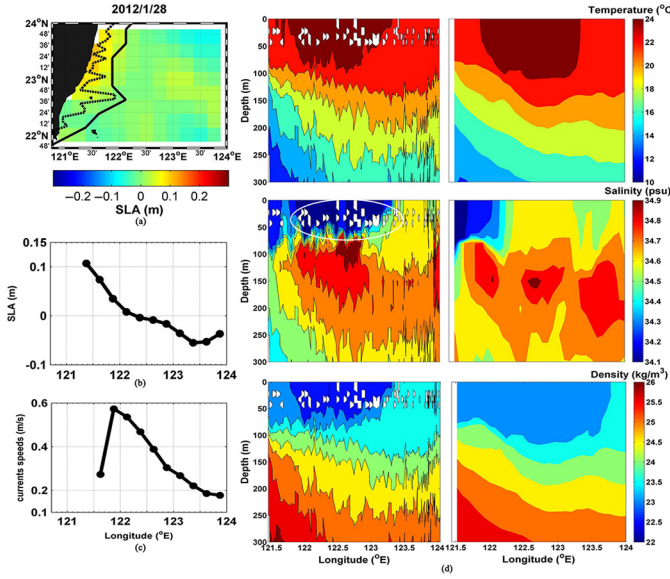


Fig. 3. Normal situation of Kuroshio east of Taiwan on January 28, 2012. (a) SLA distribution with Kuroshio axis (solid line) and left boundary (dashed line). (b) SLA values along 23°N. (c) Speeds of Kuroshio along 23°N. (d) Profiles of temperature depth (top), salinity depth (middle), and density depth (bottom) along 23°N, respectively, from glider (left) and HYCOM outputs (right).

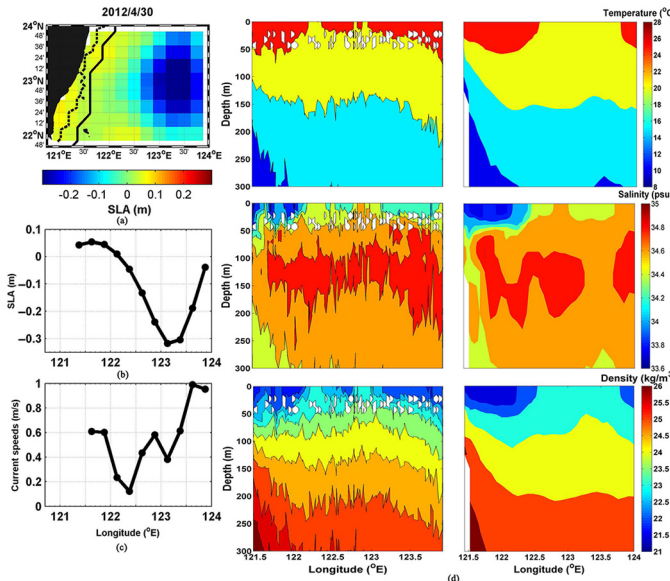


Fig. 4. Case of cold eddy impinging to the Kuroshio east of Taiwan on April 30, 2012. (a) Kuroshio axis (solid line) and left boundary (dashed line). (b) SLA value along 23°N. (c) Speeds of Kuroshio along 23°N. (d) Profiles of temperature depth (top), salinity depth (middle), and density depth (bottom) along 23°N, respectively, from glider (left) and HYCOM (right).

the temperature-depth, salinity-depth, and density-depth profiles from the spray glider data that corresponded with the HYCOM outputs. The cold eddy resulted in the pumping of low-temperature water and the uplifting of high-salinity subsurface waters. Because density and temperature exhibit inversely proportional changes, the isopycnals exhibited extensive uplifting.

TABLE II

CASES OF KUROSHIO MEANDERING EAST OF TAIWAN CAUSED BY COLD EDDY IMPINGING

Starting date of case (yyyy/mm/dd)	Duration (days)	Minimum SLA of cold eddy (m)
1994/11/02	8	-0.15
1995/01/16	11	-0.21
1995/02/07	35	-0.68
1996/01/25	17	-0.21
1996/02/24	55	-0.45
1999/04/29	19	-0.24
1999/12/02	18	-0.28
2004/01/01	34	-0.46
2004/07/01	80	-0.57
2005/03/03	20	-0.38
2009/11/03	33	-0.24
2012/11/14	12	-0.29
2013/11/17	17	-0.41

### C. Effects on Kuroshio Meandering

From 1993 to 2013, 13 cases of the Kuroshio meander occurred off east Taiwan (hereafter, KMET). The 13 cases, all of them caused by cold eddies, are listed in Table II. The KMET has occurred six times since 2002, when MODIS data became available. Because of a lack of data caused by cloud obstruction, this study ignored the case that occurred on November 17, 2013; the remaining five cases are discussed below.

The first case occurred on January 1, 2004 [Fig. 5(a)]. The Kuroshio axis can be observed on SLA maps of January 8 and 16, 2004. A cold eddy propagated northward from 20°N, 123°E, with its north edge approaching close to Orchid Island (22°N, 121.5°E; Fig. 1). The axis was shifted eastward, causing countercurrents along the coast and subsurface-water uplifting to the sea surface. The SST of the Orchid Island region was 1°C lower than that along the Kuroshio axis [Fig. 5(b)], and the chl-a concentration increased to 0.21 mg/m<sup>3</sup> at 21°N, 122.5°E [Fig. 5(c)]. The speeds of Kuroshio axis were 0.33 and 0.41 m/s at 22°N on January 8 and 16, 2004, respectively. Because of the effect of the cold eddy, the current speeds were lower than the average winter value (0.5 m/s).

Lasting up to 80 days, the longest KMET case occurred on July 1, 2004. Fig. 6(a) shows the Kuroshio axis on SLA maps for August 3, 11, 19, and 27, and for September 4, 2004. A cold eddy propagated northward and caused the Kuroshio axis to shift eastward to 123.5°E on August 3. The cold eddy induced countercurrents along the coast that lasted for 1 month. After August 19, 2004, the Kuroshio axis off southeastern Taiwan was shifted onshore by an approaching warm eddy. Even then, the Kuroshio axis off eastern Taiwan still shifted eastward because of the continued northward movement of the cold eddy. With the movement along the cold eddy path, the subsurface water was uplifted to the sea surface, causing the SST to lower [Fig. 6(b)] as the chl-a concentration increased to 0.37 mg/m<sup>3</sup> [Fig. 6(c)].

Another KMET case occurred in 2005. Fig. 7(a) shows the Kuroshio axis on SLA maps of March 13, 20, and 29, 2005. A cold eddy propagated northwestward from 21°N, 123.5°E to 22°N, 122.5°E and pushed the Kuroshio, causing its axis to shift eastward. After the cold eddy weakened gradually on

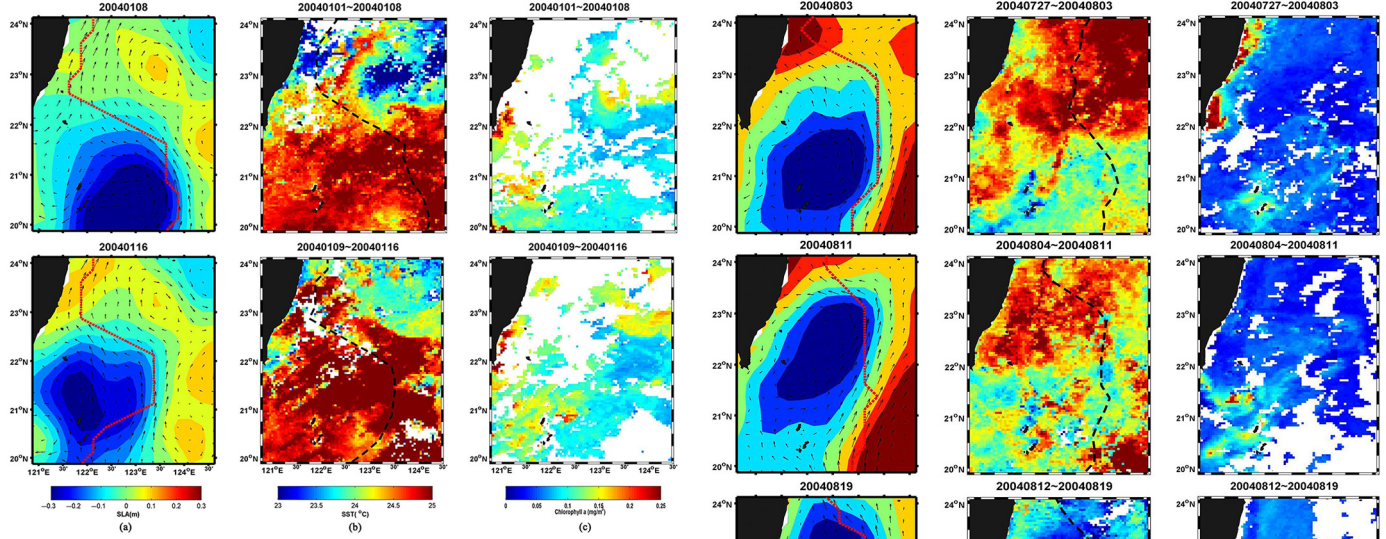


Fig. 5. Effects on Kuroshio meandering from January 1–16, 2004. (a) Kuroshio axis (red line) and SLA (background). (b) 8-day average values of Kuroshio axis (black dashed line) and SST (background). and (c) 8-day average values of chl-a; blank represents no data.

March 20 [Fig. 7(b)], the Kuroshio axis returned to its original path. On March 29, the cold eddy shrank to a small size near the southeastern coast of Taiwan. The subsurface cold water was uplifted to the sea surface. The SST of the coastal region was  $2^{\circ}\text{C}$  [Fig. 7(b)], lower than that along the Kuroshio axis, and the chl-a concentration increased to  $0.54 \text{ mg/m}^3$  [Fig. 7(c)]. The speeds of the Kuroshio axis were 0.38, 0.59, and  $0.60 \text{ m/s}$  at  $22^{\circ}\text{N}$  on March 13, 20, and 29, respectively; speeds much lower than the average spring value of  $0.6 \text{ m/s}$ . As the influence of the eddy weakened, the speed of the Kuroshio returned to the average value.

Fig. 8 shows a case that occurred with two cold eddies in fall 2009. Fig. 8(a) shows the Kuroshio axis on SLA maps of November 6, 12, and 19, 2009. The Kuroshio axis was shifted eastward to  $123^{\circ}\text{E}$  because of the two eddies at  $22^{\circ}\text{N}$  and  $23^{\circ}\text{N}$ , respectively. The SST of the cold eddy region was  $2^{\circ}\text{C}$  lower than that along the Kuroshio path [Fig. 8(b)], and the chl-a concentration increased to  $0.45 \text{ mg/m}^3$  [Fig. 8(c)]. The speed at the Kuroshio axis was  $0.37 \text{ m/s}$  at  $23^{\circ}\text{N}$  on November 6, 2009 [Fig. 8(a)], which was only half of the average value in fall ( $0.75 \text{ m/s}$ ). Fig. 9 shows another case in fall 2012. The Kuroshio axis on the SLA map is shown in Fig. 9(a). The SST of the cold eddy region was  $3^{\circ}\text{C}$  lower than that along the Kuroshio path [Fig. 9(b)], and the chl-a concentration was up to  $0.2 \text{ mg/m}^3$  [Fig. 9(c)]. The average speed at the Kuroshio axis was only  $0.28 \text{ m/s}$  on November 25. Fig. 10 shows the KMET case in 2013. The cold eddy shifted the Kuroshio axis to  $123^{\circ}\text{E}$  around  $23^{\circ}\text{N}$ . There were no SST and chl-a data available because of cloud obstruction.

The remaining seven KMET cases accessed from altimeter data between 1993 and 2002 are shown in Fig. 11. Cold eddies shifted the Kuroshio axis eastward between  $121^{\circ}\text{E}$  and  $123^{\circ}\text{E}$  in all cases. The eastward most shift of the Kuroshio axis, farther than  $123^{\circ}\text{E}$  at  $23^{\circ}\text{N}$ , occurred on February 22, 1995. The absence of SST and chl-a data made it difficult

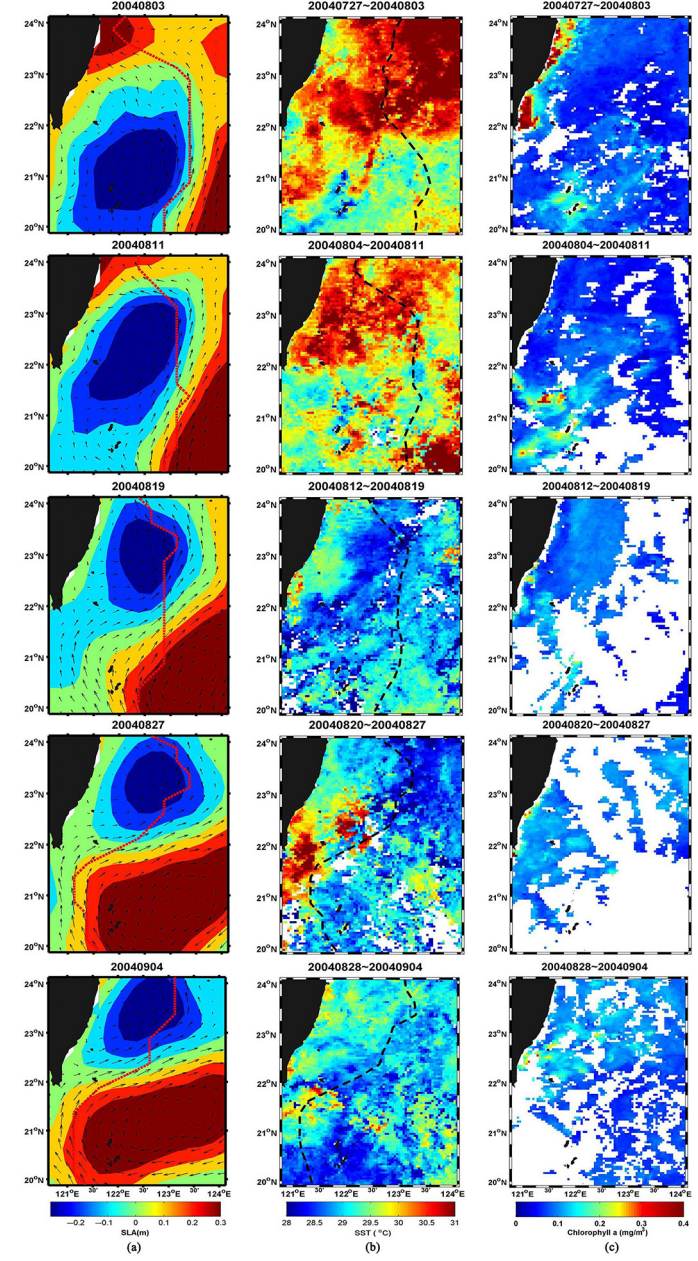


Fig. 6. Same as Fig. 5, but from August 3 to September 4, 2004.

to further explain how the cold eddy affected the surrounding environment. On December 10, 1999, a compelling case occurred in which a large eddy was near the east of Taiwan. According to the theory of geostrophic balance, the maximum speed should occur at the maximum gradient of the eddy edge. However, in this case, the Kuroshio axis penetrated the eddy. More information is necessary to interpret this phenomenon

#### IV. DISCUSSION AND CONCLUSION

The KMET occurred 13 times from 1993 to 2013. All cases were caused by westward or northward moving cold eddies when they propagated to the east of Taiwan. Table III lists the statistical properties of these cold eddies. The average duration

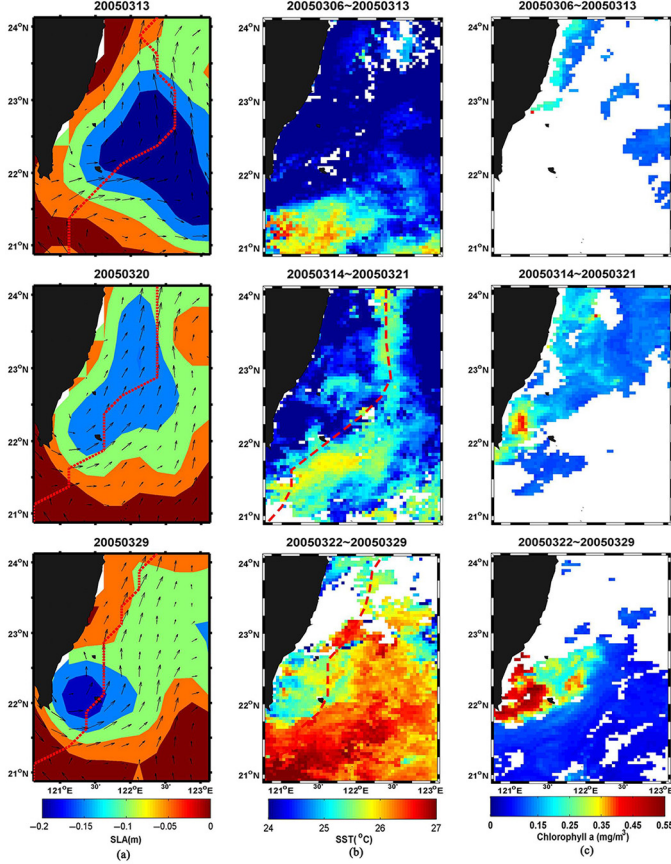


Fig. 7. Same as Fig. 5, but from March 13–29, 2005.

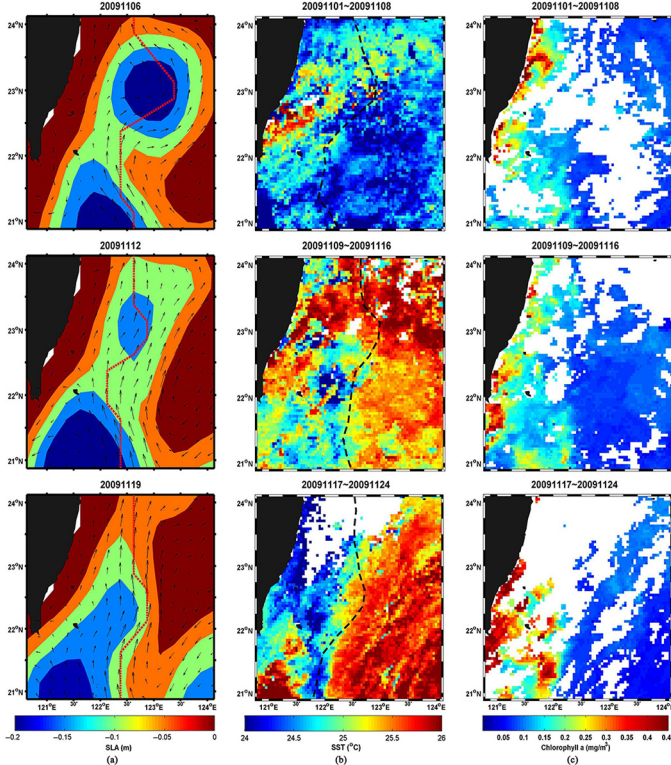


Fig. 8. Same as Fig. 5, but from November 6–19, 2009.

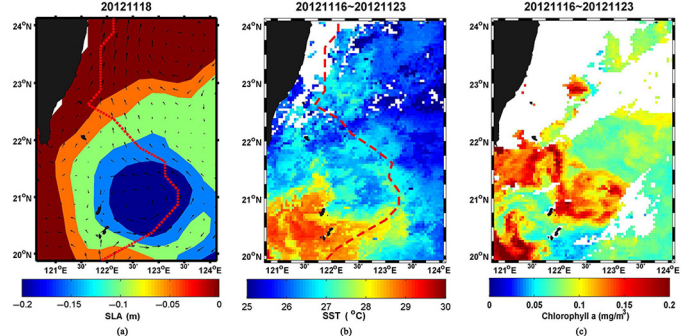


Fig. 9. Same as Fig. 5, but from November 16–23, 2012.

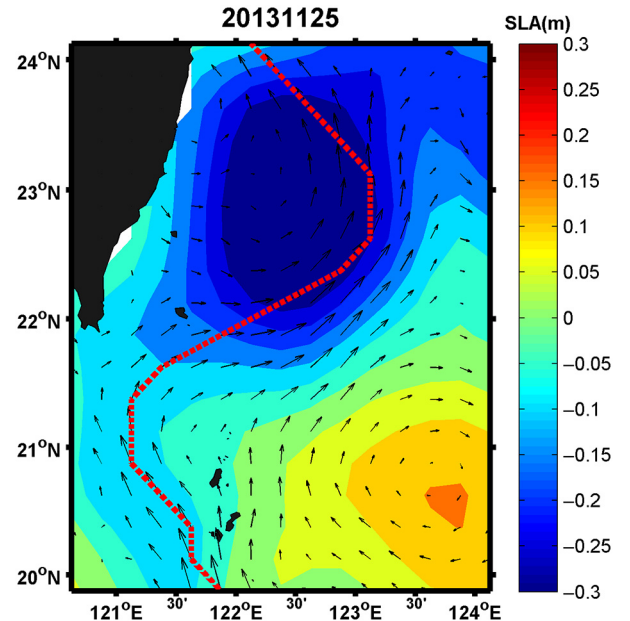


Fig. 10. Effects on Kuroshio meandering on November 25, 2013. The Kuroshio axis (red line) and the SLA (background).

of the meanderings was  $27 \pm 20$  days, and the maximum duration was 80 days. The mean propagating speeds of the eddies were between 0.01 and 0.14 m/s. The maximum diameter of a cold eddy, which is defined as the maximum distance across the eddy center in the closed contours of the eddy, was 269 km. Table IV lists the effects of cold eddies on the KMET and Kuroshio axis speeds. The farthest position of the Kuroshio axis was at 123.875°E on January 1, 2004, which is approximately 270 km from the average Kuroshio axis. Although it was not the largest eddy of the 13 cases, it exhibited the largest eddy kinetic energy (EKE), which is calculated using

$$\text{EKE} = (u^2 + v^2)/2. \quad (4)$$

The mean shifted distance from the average axis was  $155 \pm 56$  km. Figs. 12 and 13 show scatter plots of the shifting distance of the Kuroshio with the EKE and maximum diameter of the eddy, respectively. The diameter rather than the EKE showed a more favorable correlation with the eddy shifting distance. Not considering the only westward-propagating case (February 24, 1996), which was generated at a local

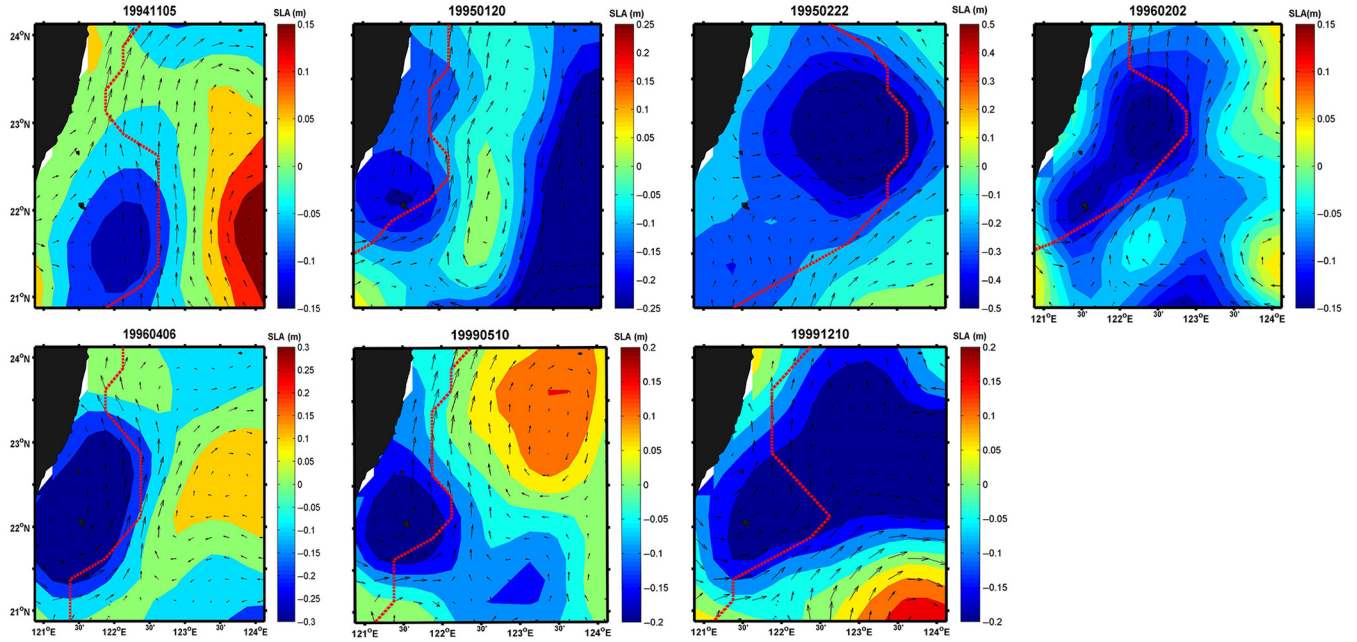


Fig. 11. Effects on Kuroshio meandering between 1993 and 2002. The red line represents the Kuroshio axis. The date on each figure is the date of maximum shifting position of the Kuroshio axis.

TABLE III  
STATISTICAL PROPERTIES OF COLD EDDY ON KMET

Starting date of case (yyyy/mm/dd)	Propagation direction	Mean propagating speed (m/s)	Maximum diameter (km)	Mean SLA (m)	Maximum EKE (cm <sup>2</sup> /s <sup>2</sup> )
1994/11/02	WNW	0.09	129	-0.14±0.02	184
1995/01/16	NW	0.01	103	-0.19±0.02	350
1995/02/07	NNW	0.08	269	-0.55±0.10	1078
1996/01/25	WNW	0.07	230	-0.23±0.05	390
1996/02/24	W	0.01	155	-0.34±0.07	1169
1999/04/29	NW	0.11	129	-0.27±0.07	689
1999/12/02	NNE	0.02	180	-0.26±0.03	399
2004/01/01	NW	0.14	235	-0.33±0.11	1270
2004/07/01	NNW	0.09	237	-0.39±0.10	841
2005/03/03	NW	0.09	180	-0.27±0.09	373
2009/11/03	WNW	0.14	154	-0.25±0.10	286
2012/11/14	N	0.05	221	-0.25±0.04	329
2013/11/17	NW	0.03	205	-0.36±0.06	625

TABLE IV  
EFFECTS OF COLD EDDY ON KMET

Date of most eastward position occurred (yyyy/mm/dd)	Most eastward position of KMET	Shifting distance (km)	Kuroshio axis speed (m/s)
1994/11/04	22.375°N 122.625°E	103	0.54
1995/01/19	22.375°N 122.375°E	77	0.92
1995/02/19	22.625°N 123.875°E	218	0.67
1996/01/25	23.625°N 123.875°E	187	0.41
1996/04/04	22.625°N 122.375°E	71	1.10
1999/04/29	21.875°N 122.625°E	149	0.74
1999/12/10	22.125°N 122.625°E	121	0.52
2004/01/11	21.875°N 123.875°E	270	0.43
2004/08/06	22.625°N 123.375°E	168	1.08
2005/03/10	22.375°N 122.875°E	141	0.50
2009/11/06	23.125°N 123.375°E	149	0.37
2012/11/16	21.875°N 123.125°E	191	0.24
2013/11/20	22.625°N 123.375°E	166	0.61
<b>Mean±std</b>		<b>155±56</b>	<b>0.63±0.27</b>

The shifted distance is the distance of Kuroshio axis shifted away from the average axis at the same latitude and season.

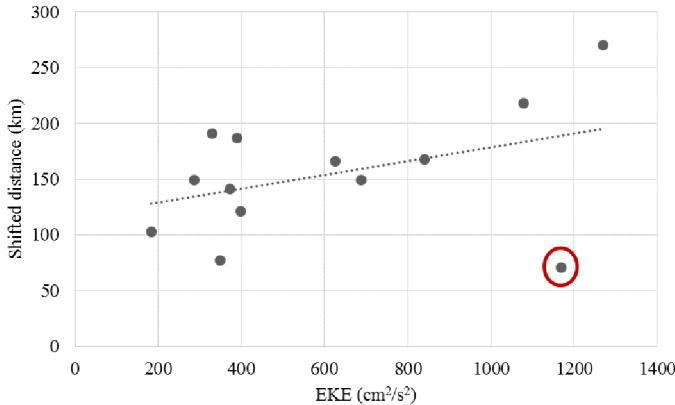


Fig. 12. Scatter plot of EKE and shifted distance of eddy. The determination coefficient ( $R^2$ ) is 0.16. If the western propagating case (red circle) was removed,  $R^2$  is increased to 0.59.

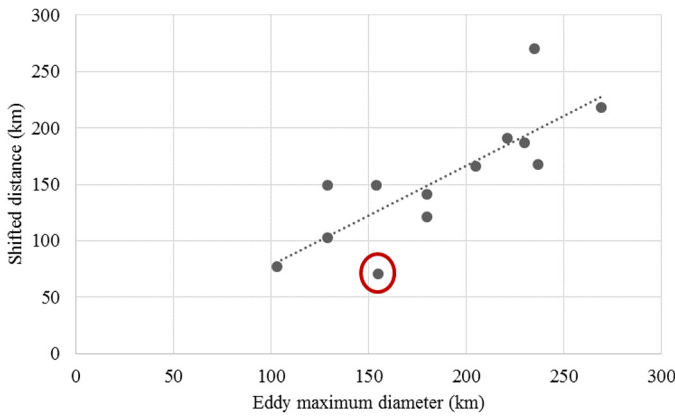


Fig. 13. Scatter plot of eddy maximum diameter and shifted distance of eddy.  $R^2$  is 0.65. If the western propagating case (red circle) was removed,  $R^2$  is increased to 0.68.

position and moved only slightly (moving speed  $< 0.01$  m/s), markedly improves the relationship between the shifting distance and the maximum diameter, implying that the shifting position is affected by the size of the cold eddy. Under the circumstances of a cold eddy, the mean speed of the Kuroshio axis drops to 0.63 m/s, which is approximately 84% of the seasonal average. Derived from MODIS data, the SST in the Kuroshio region is 1 – 3 °C higher than that in the cold eddy region. The chl-a concentration in the cold eddy region is 0.21–0.54 mg/m<sup>3</sup>. These values are 2.2- to 5.7-fold higher than those of the seasonal average.

In summary, this study investigated the effects of cold eddies on the Kuroshio meander and changes in its surface water properties east of Taiwan. Not only cold eddies but also warm eddies can cause Kuroshio meandering. The warm eddy effects are considerably more complex and must be studied in the future. The present study contributes to the analysis of the impacts of cold eddies on the entire depth of the Kuroshio east of Taiwan.

#### ACKNOWLEDGMENT

The authors would like to thank the associate editor and the anonymous reviewers for their valuable suggestions and

comments. Glider data are provided by National Oceanographic Data Center of NOAA. MODIS data are produced with the NASA's OceanColor Web, developed and maintained by the Ocean Biology Distributed Active Archive Center (OB.DAAC). Altimetry data are provided by the Archiving Validation and Interpretation of Satellite Data in Oceanography (AVISO), the Centre National d'Études Spatiales (CNES) of France. HYCOM model outputs are provided by HYCOM consortium, which is sponsored by the National Ocean Partnership Program (NOPP), as part of the U.S. Global Ocean Data Assimilation Experiment (GODAE).

#### REFERENCES

- [1] B. Qiu, "Seasonal eddy field modulation of the north pacific subtropical counter-current: TOPEX/Poseidon observations and theory," *J. Phys. Oceanogr.*, vol. 29, pp. 2471–2486, Oct. 1999.
- [2] D. Roemmich and J. Gilson, "Eddy transport of heat and thermocline waters in the north pacific: A key to interannual/decadal climate variability?," *J. Phys. Oceanogr.*, vol. 31, pp. 675–687, Mar. 2001.
- [3] C. Hwang, C. R. Wu, and R. Kao, "TOPEX/Poseidon observations of mesoscale eddies over the subtropical counter-current: Kinematic characteristics of an anticyclonic eddy and a cyclonic eddy," *J. Geophys. Res.*, vol. 109, Aug. 2004, doi: 10.1029/2003JC002026.
- [4] I. I. Lin, C. C. Wu, K. A. Emanuel, I. H. Lee, C. R. Wu, and I. F. Pun, "The interaction of supertyphoon maemi (2003) with a warm ocean eddy," *Mon. Weather Rev.*, vol. 133, pp. 2635–2649, Sep. 2005.
- [5] R. C. Lien *et al.*, "Modulation of kuroshio transport by mesoscale eddies at the luzon strait entrance," *J. Geophys. Res.*, vol. 119, pp. 2129–2142, Apr. 2014.
- [6] Y. Yang, C.-T. Liu, J.-H. Hu, and M. Koga, "Taiwan current (kuroshio) and impinging eddies," *J. Oceanogr.*, vol. 55, pp. 609–617, Oct. 1999.
- [7] W. E. Johns, T. N. Lee, D. X. Zhang, R. Zantopp, C. T. Liu, and Y. Yang, "The kuroshio east of taiwan: Moored transport observations from the WOCE PCM-1 array," *J. Phys. Oceanogr.*, vol. 31, pp. 1031–1053, Apr. 2001.
- [8] D. X. Zhang, T. N. Lee, W. E. Johns, C. T. Liu, and R. Zantopp, "The kuroshio east of taiwan: Modes of variability and relationship to interior ocean mesoscale eddies," *J. Phys. Oceanogr.*, vol. 31, pp. 1054–1074, Apr. 2001.
- [9] Y. C. Kuo and C. S. Chern, "Numerical study on the interactions between a mesoscale eddy and a western boundary current," *J. Oceanogr.*, vol. 67, pp. 263–272, Jun. 2011.
- [10] D. Takahashi, X. Y. Guo, A. Morimoto, and S. Kojima, "Biweekly periodic variation of the kuroshio axis northeast of taiwan as revealed by ocean high-frequency radar," *Cont. Shelf. Res.*, vol. 29, pp. 1896–1907, Aug. 2009.
- [11] S. Guinehut, C. Coatanoan, A. L. Dhomps, P. Y. Le Traon, and G. Larnicol, "On the use of satellite altimeter data in argo quality control," *J. Atmos. Oceanic. Technol.*, vol. 26, pp. 395–402, Feb. 2009.
- [12] Y. S. Soong, J. H. Hu, C. R. Ho, and P. P. Niiler, "Cold-core eddy detected in south china sea," *EOS Trans. Amer. Geophys. Union*, vol. 76, pp. 345–347, Aug. 1995.
- [13] D. B. Chelton, M. G. Schlax, R. M. Samelson, and R. A. de Szoeke, "Global observations of large oceanic eddies," *Geophys. Res. Lett.*, vol. 34, Aug. 2007, doi: 10.1029/2007GL030812.
- [14] D. B. Chelton, M. G. Schlax, and R. M. Samelson, "Global observations of nonlinear mesoscale eddies," *Prog. Oceanogr.*, vol. 91, pp. 167–216, Oct. 2011.
- [15] Q. A. Zheng *et al.*, "Satellite altimeter observations of nonlinear rossby eddy-kuroshio interaction at the luzon strait," *J. Oceanogr.*, vol. 67, pp. 365–376, Aug. 2011.
- [16] Y. H. Cheng, C. R. Ho, Q. N. Zheng, and N. J. Kuo, "Statistical characteristics of mesoscale eddies in the north pacific derived from satellite altimetry," *Remote Sens.*, vol. 6, pp. 5164–5183, Jun. 2014.
- [17] R. Y. Setiawan and A. Habibi, "Satellite detection of summer chlorophyll-a bloom in the gulf of tomini," *IEEE J. Sel. Topics Appl. Earth Observ. Remote Sens.*, vol. 4, no. 4, pp. 944–948, Dec. 2011.
- [18] R. Y. Setiawan and H. Kawamura, "Summertime phytoplankton bloom in the south Sulawesi Sea," *IEEE J. Sel. Topics Appl. Earth Observ. Remote Sens.*, vol. 4, no. 1, pp. 241–244, Mar. 2011.

- [19] C. Dong, F. Nencioli, Y. Liu, and J. C. McWilliams, "An automated approach to detect oceanic eddies from satellite remotely sensed sea surface temperature data," *IEEE Geosci Remote Sens. Lett.*, vol. 8, no. 6, pp. 1055–1059, Nov. 2011.
- [20] Y. Gu, J. Pan, and P. Li, "Remote sensing studies of an upwelling jet in guangdong coastal water," *IEEE J. Sel. Topics Appl. Earth Observ. Remote Sens.*, vol. 8, no. 1, pp. 160–170, Jan. 2015.
- [21] R. K. Sarangi, M. K. Mishra, and P. Chauhan, "Remote sensing observations on impact of phailin cyclone on phytoplankton distribution in northern bay of bengal," *IEEE J. Sel. Topics Appl. Earth Observ. Remote Sens.*, vol. 8, no. 2, pp. 539–549, Feb. 2015.
- [22] R. D. Ray, "Spectral analysis of highly aliased sea-level signals," *J. Geophys. Res.*, vol. 103, pp. 24991–25003, Oct. 1998.



**Po-Chun Hsu** (S'15) received the B.S. and M.S. degrees in marine environmental informatics from the National Taiwan Ocean University, Keelung, Taiwan, in 2012 and 2013, respectively. He is currently working toward the Ph.D. degree in marine of environmental informatics at the Laboratory of Environmental Remote Sensing, National Taiwan Ocean University.

His research interests include high-resolution remote-sensing application, satellite and physical oceanography, climate dynamics, and ocean monitoring using remote-sensing technology.



**Chen-Chih Lin** received the Ph.D. degree in marine environmental informatics from the National Taiwan Ocean University, Keelung, Taiwan, in 2014.

Her research interests include climate variability and marine environment change with remote-sensing data.



**Shih-Jen Huang** received the Ph.D. degree in space science from the National Central University, Chung-Li, Taiwan, in 2002.

He is an Assistant Professor with the National Taiwan Ocean University, Keelung, Taiwan. His research interests include remote sensing, atmospheric correction, and ocean dynamics.



**Chung-Ru Ho** received the Ph.D. degree in applied ocean science from the University of Delaware, Newark, DE, USA, in 1994.

He is a Professor with the National Taiwan Ocean University, Keelung, Taiwan, and Deputy Director General of National Museum of Marine Science and Technology, Keelung, Taiwan. His research interests include eddy-current interaction, typhoon-ocean interaction, global change, and ocean renewable energy.

Dr. Ho is currently serving as a National Committee Member of Committee on Space Research (COSPAR) and International Union of Geodesy and Geophysics (IUGG). He was the Editor-in-Chief for the *Journal of Marine Science and Technology*, and a Guest Editor for different journals, including *Advances in Meteorology*, *Atmospheric Research*, *Journal of Marine Science and Technology*, and *Journal of Photogrammetry and Remote Sensing*.